Nuclear Physics **A412** (1984) 159–188

FOUR-NUCLEON TRANSFER WITH THE $^{32}S(^{16}O, ^{12}C)^{36}Ar$ REACTION

A. BECKER, C. ALDERLIESTEN, E. A. BAKKUM, C. P. M. VAN ENGELEN and R. KAMERMANS

Fysisch Laboratorium, Rijksuniversiteit Utrecht, PO Box 80000, 3508 TA Utrecht, The Netherlands

Received 2 May 1983
(Revised 2 August 1983)

Abstract: Angular distributions have been measured for the $^{32}S(^{16}O, ^{12}C)^{36}Ar$ reaction at 45.5 MeV leading to excited states between $E_x = 0$ and 8 MeV. Experimental cross sections are compared with exact finite-range DWBA calculations in combination with extensive shell-model calculations, which include sd- and fp-shell configurations. Transitions to low-energy positive-parity states and bound negative-parity states are well reproduced. The calculations, however, fail to describe some high-energy positive-parity states. Calculations with a complete cluster expansion for the four transferred nucleons give about 50 % larger cross sections, but can not explain the observed discrepancies. Possible interference of reaction processes other than direct α-transfer and special structure effects are discussed.

E NUCLEAR REACTIONS $^{32}S(^{16}O, ^{12}C)$, $E = 45.5$ MeV; measured $\sigma(E(^{12}C), \theta)$. Magnetic spectrograph, gas-ionization chamber. Exact finite-range DWBA analysis, shell-model calculations, full cluster expansion.

1. Introduction

One of the reasons for studying reactions with light heavy ions like ^{16}O or ^{12}C at low incident energies has been the possibility of obtaining information on multi-nucleon correlations in nuclei. In order to extract structure information from the data, the reaction mechanism ought to be understood rather well. During the last few years considerable experimental effort has been invested to obtain detailed angular distributions and excitation functions especially for elastic scattering with oxygen or carbon projectiles. Recent reviews of the salient features of these data can be found in refs. [1,2]). Although a complete picture of all observed scattering phenomena has still not emerged, the main characteristics are now understood reasonably well.

While elastic scattering from heavy targets or at high incident energies appears to be of a diffractive nature (Fresnel or Fraunhofer type), which requires the use of strongly absorbing optical-model potentials [3–5]), the scattering from lighter targets (sd-shell or p-shell) at energies not too far above the Coulomb barrier

shows refractive properties which can only be described with surface-transparent potentials [6-9]). Such potentials are weakly absorbing in the exterior part of the nuclear interaction region, which allows the occurrence of orbiting for the grazing partial waves. This surface transparency is especially pronounced for scattering systems involving nuclei which are composed of α-particles, where strong oscillations of the angular distributions for elastic scattering beyond the grazing angle have been observed. Also the strong backward rise of the angular distributions observed for several systems [10-14]), together with the resonance-like structures found in 180° excitation functions [12-16]), seems to require surface transparency, although this is not sufficient to give a satisfactory description of the data.

Evidence for surface transparency has also been found in α-transfer reactions like (^{16}O, ^{12}C) on ^{24}Mg and ^{28}Si [refs. [17,18])], where the strongly oscillating angular distributions indicate the dominance of only a few partial waves. In addition, for these reactions, backward rising angular distributions and structured excitation functions at backward angles have been found [12-14]), similar although apparently not correlated to the elastic scattering. While for the ^{24}Mg(^{16}O, ^{12}C)^{28}Si reaction strong structures have also been found in the forward-angle excitation functions [19-22]), these are already much weaker for ^{28}Si(^{16}O, ^{12}C)^{32}S [ref. [23])]. At present no model exists in which all these phenomena can be described simultaneously; for reviews see refs. [6,24]). However, angular distributions in the forward hemisphere generally can be described successfully by DWBA calculations with surface-transparent potentials and the extracted relative spectroscopic factors are energy independent and in reasonable agreement with values extracted from (^{6}Li, d) data and with shell-model or SU(3) calculations in the few cases for which such calculations have been performed.

In the present work the ^{32}S(^{16}O, ^{12}C)^{36}Ar reaction at 45.5 MeV incident energy was investigated with sufficient energy resolution for the ^{12}C ejectiles (120–150 keV) to extract angular distributions for most of the populated states in ^{36}Ar up to 8 MeV in excitation energy. The data are compared with exact finite-range DWBA calculations with detailed shell-model calculations of the four-nucleon spectroscopic amplitudes. The latter include contributions of fp-shell admixtures in the wave functions. It was found that the shape of some angular distributions could not be described with standard DWBA calculations, while calculations with excited four-nucleon clusters produced shapes in much better agreement with these data. Therefore extensive calculations have been performed with the four nucleons transferred in excited configurations. The calculated strength of such contributions was, however, not sufficient to dominate those specific transitions in the ^{32}S(^{16}O, ^{12}C)^{36}Ar reaction, although they are in general not negligible. The failure to reproduce these angular distributions may be evidence for the presence of other reaction mechanisms than direct single-step "α-transfer", or of special structure properties of these states.

2. Data acquisition and reduction

2.1. EXPERIMENTAL PROCEDURE

The (^{16}O, ^{12}C) reaction on ^{32}S was studied with a 45.5 MeV beam of $^{16}O^{6+}$ ions produced by the 7 MV EN tandem accelerator in Utrecht with beam currents up to 1 μA. The angular spread of the beam and the target spot size were optimized to give a minimum kinematical contribution to the energy resolution of the ^{12}C ejectiles. Targets consisted of about 70 $\mu g/cm^2$ ZnS (natural S) evaporated on silver backings of about 70 $\mu g/cm^2$ thickness. They were regularly replaced in order to keep the carbon and oxygen contaminations within acceptable limits. It appeared that the heat dissipation of the beam in the target foils introduced tensions which caused inhomogeneities in the target thickness around the beam spot, which resulted in small tails on the peaks in the ^{12}C spectra.

The reaction products were momentum analyzed in an Enge split-pole spectrograph and detected in a gas-ionization chamber [25]) of 30 cm effective length along the focal plane of the spectrograph. The detector was filled with isobutane at a pressure of 50 Torr, which was sufficient to provide a good element separation of the reaction products. The 1.2 mm intrinsic position resolution corresponds to 65 keV for 40 MeV ^{12}C and is small compared to the total energy resolution of 120–150 keV which was largely determined by energy losses in the target.

In order to avoid too high count rates in the detector it was necessary to prevent the elastically scattered ^{16}O ions to enter the detector. This was accomplished by choosing the magnetic field of the spectrograph such that one of the interfering ^{16}O charge states fell just outside the range of the detector while the next higher charge state was stopped in a movable brass plate blocking 3 cm of the detector range. For this reason both the 5+ and 6+ charge states of the ^{12}C ions had to be measured in order to cover the whole range of excitation energies (0–8 MeV) in ^{36}Ar. Special provisions had to be made for the measurements at the smallest scattering angles (θ_{lab} = 2°–5°) in order to reduce the intense background of ^{16}O ions produced by slit-scattering and by scattering from rest-gas molecules in the spectrograph. For these measurements a 41 μm thick mylar foil was mounted in the entrance window of the detector which was just thick enough to stop the ^{16}O ions, while the ^{12}C ions retained sufficient energy to be detected in the ionization chamber operated at a pressure of 15 Torr.

Angular distributions for both the 5+ and 6+ ^{12}C ejectiles were measured in 1.5° steps from θ_{lab} = 2° to 35°. The angular acceptance of the spectrograph was $\Delta\theta$ = 1.5° with a solid angle of 1.2 msr. Complete angular distributions were also taken with carbon and NiO targets in order to correct the spectra for impurities resulting from C- and O-contaminants in the S-targets. The target composition was constantly monitored by measuring the elastic scattering in a silicon detector placed at a fixed angle of θ_{lab} = 30° or 40°. For the purpose of absolute normalization ^{16}O elastic scattering was measured at forward angles, while also the

charge state distributions of ^{12}C and ^{16}O ions were measured over the energy range of interest.

All primary signals from the detector were stored on magnetic tape by a PDP-11/34 computer. The dead-time for the whole set-up was determined with an electronic pulse generator. The particle identification and the construction of momentum spectra for the ^{12}C ions were performed off-line with a PDP-11/70 computer.

2.2. DATA ANALYSIS

An example of a $^{12}C^{5+}$ spectrum measured at $\theta_{lab} = 5°$ is shown in fig. 1. From this figure it is clear that the rather high level density in ^{36}Ar above $E_x = 4$ MeV makes a careful analysis necessary. Most of the known natural-parity levels of ^{36}Ar up to $E_x = 8$ MeV are populated. Also the 4.44 MeV state in the ^{12}C ejectile with a Doppler-broadened peak shape is observed. The spectra are further complicated by the presence of impurity peaks from reactions on ^{12}C and ^{16}O, which differ in shape from the Ar peaks, because they are not well focussed. In view of this

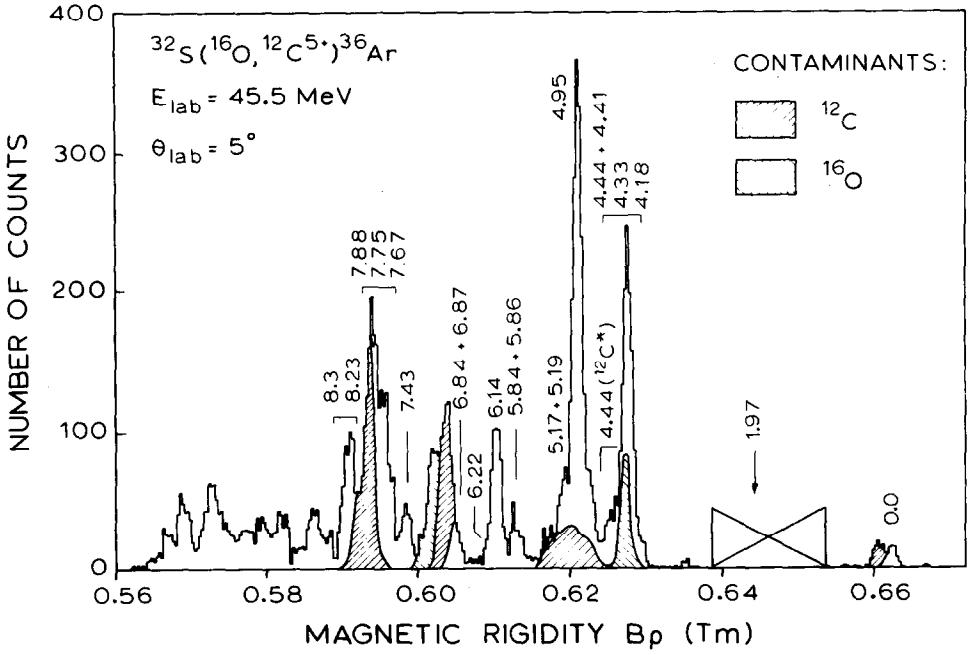

Fig. 1. Spectrum of $^{12}C^{5+}$ ions emitted in the reaction $^{32}S(^{16}O, ^{12}C)^{36}Ar$. The peaks are labelled by the excitation energies of the corresponding states in ^{36}Ar. Hatched areas indicate impurity peaks resulting from the reactions $^{12}C(^{16}O, ^{12}C)^{16}O$ and $^{16}O(^{16}O, ^{12}C)^{20}Ne$. The part of the spectrum indicated by a cross was blocked in order to stop elastically scattered ^{16}O ions.

complexity the procedure followed in fitting the spectra will be discussed in some detail.

It was found possible to fix the positions of all peaks, which were calculated from the reaction kinematics including energy losses in the target. Only the offset in the (linear) calibration function was allowed to vary smoothly over the spectrum range. A small constant background was applied in order to correct for products from the reaction on other S-isotopes. For the shapes of the Ar peaks a gaussian was taken with a small satellite of the same shape to account for the target inhomogeneities discussed in subsect. 2.1. The three parameters of this function were kept constant over the range of each spectrum. The peaks from the ^{12}C and ^{16}O contaminants were analyzed with a block function having a width calculated from the focussing properties of the spectrograph and folded with the Ar peak shape. Also the Doppler shapes of the peaks corresponding to ^{12}C ejectiles excited in the reaction on ^{32}S and on ^{12}C were calculated correctly, taking into account the recoil from the emitted γ-rays and the E2 angular correlation of the γ-rays. The contents of the contaminant peaks could be fixed by means of the spectra measured with C and NiO targets and the contents of the target monitor. Therefore each spectrum was fitted with essentially four free parameters apart from the contents of the Ar peaks. A result of this procedure for part of the spectrum of fig. 1 is shown in fig. 2, which displays the contributions of all individual transitions to a complex group.

Relative cross sections were determined by normalizing each run with the contents of the target monitor and the measured (energy-dependent) charge-state fractions. The absolute normalization with an estimated accuracy of 20% was obtained by comparing ^{16}O elastic scattering measured at forward angles to existing data [26]) and optical-model calculations.

2.3. PRESENTATION OF THE DATA

All angular distributions resulting from the analysis discussed above are presented in figs. 3–5. The curves through the data points are DWBA calculations which will be discussed in sects. 3 and 4.

The transitions to the ^{36}Ar ground state and the $E_x = 1.97$ MeV $J^\pi = 2^+$ state are well isolated from other transitions. Their angular distributions show the expected strongly oscillating shape which indicates the need for surface transparency in the nucleus-nucleus interaction. The distinction between the $L = 0$ and $L = 2$ character of these angular distributions is also clear, especially at forward angles. The data for these two states are in reasonable agreement with those of ref. [26]).

From the group of levels between 4.0 and 4.5 MeV the strongly populated 4.18 MeV 3^- state and the 4.33 MeV state, assigned $J^\pi = (0\text{–}2)^+$ [ref. [27])], are well resolved. In the $L = 3$ angular distribution the oscillations are already much

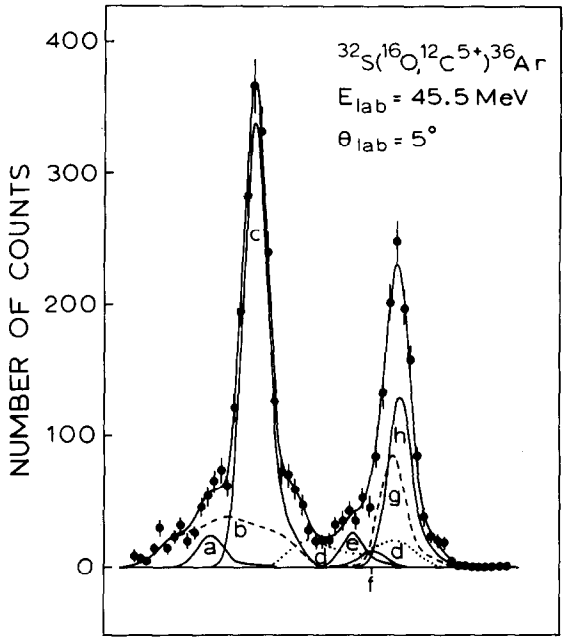

Fig. 2. Decomposition of part of the spectrum of fig. 1, covering excitation energies in ^{36}Ar from E_x = 3.5 to 5.5 MeV. The contributions from all individual transitions are indicated: (a) ^{36}Ar (5.17 MeV + 5.19 MeV); (b) ^{12}C (4.44 MeV), ^{16}O (g.s.); (c) ^{36}Ar (4.95 MeV); (d) ^{12}C (4.44 MeV), ^{36}Ar (g.s.); (e) ^{36}Ar (4.41 + 4.44 MeV); (f) ^{36}Ar (4.33 MeV); (g) ^{20}Ne (1.63 MeV); (h) ^{36}Ar (4.18 MeV).

damped due to the many contributing magnetic substates [17]). The strong similarity of the angular distributions for the ground-state transition and the transition to the 4.33 MeV state (fig. 3) leads to a $J^\pi = 0^+$ assignment for the latter state. The transitions to the 4.41 MeV 4^+ and the 4.44 MeV 2^+ states (fig. 4), analyzed as a doublet, are so weak that the extracted cross sections may only be regarded as an upper limit. The ^{12}C(4.44 MeV) ejectile excitation in the ^{32}S(^{16}O, ^{12}C*)^{36}Ar reaction is rather strong, although the accuracy of the angular distribution for this state is not very good (fig. 3).

The group of levels around E_x = 5 MeV contains the 4.95 MeV 2^+ state which is most strongly populated. The similarity of its angular distribution with that for the 1.97 MeV 2^+ state is evident from fig. 3. The angular distribution for the close doublet consisting of the 5.17 MeV and 5.19 MeV states is shown in fig. 4. On top of the smooth (calculated) shape for the 5.17 MeV 5^- angular distribution pronounced oscillations are observed, especially at forward angles, suggesting an $L = 0$ character for the transition to the 5.19 MeV level, to which $J^\pi = (0^+ - 3^-)$ was assigned [27]). The 4.97 MeV 2^- state, expected to be weakly populated because of its unnatural parity, was not considered in the analysis.

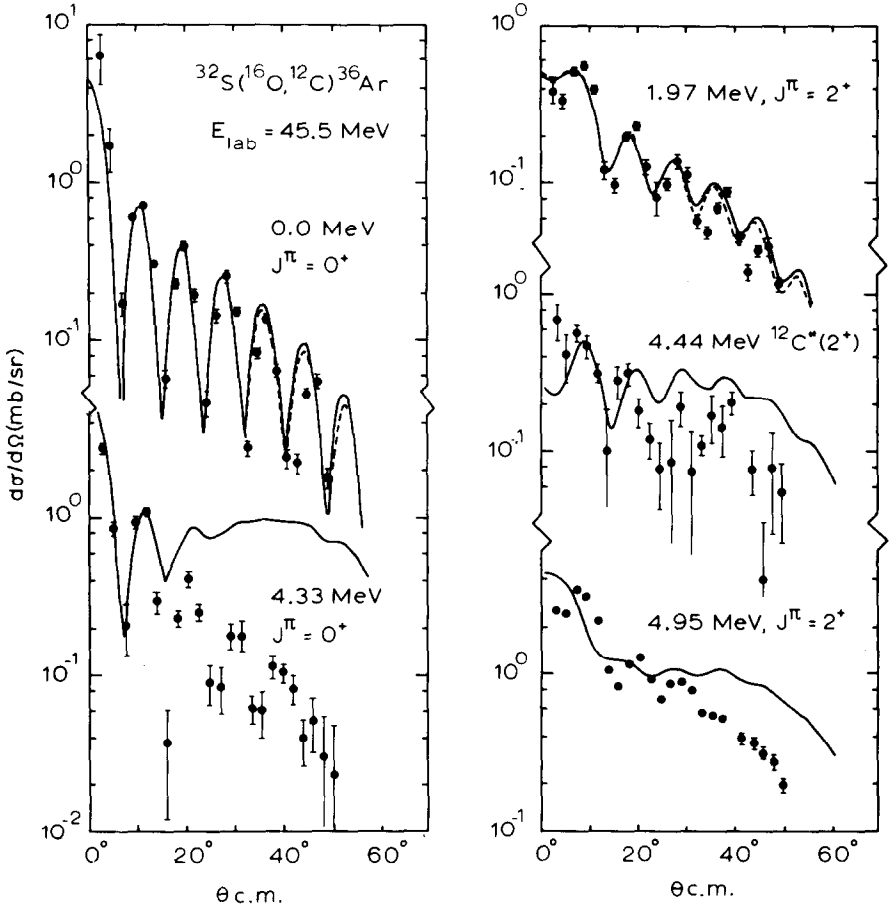

Fig. 3. Angular distributions for $J^\pi = 0^+$ states (left part) and for $J^\pi = 2^+$ states (right part) observed in the reaction $^{32}S(^{16}O, ^{12}C)^{36}Ar$ at $E_{lab} = 45.5$ MeV. The curves are results of DWBA calculations which include the full cluster expansion for the four transferred nucleons (see sect. 4). Shell-model wave functions TH1 (dashed curves) and TH2 (full curves) were used to calculate the spectroscopic amplitudes (see subsect. 3.4).

The group of levels around 6 MeV consists of two doublets, of which that containing the strongly populated 6.14 MeV state and the weaker 6.22 MeV 5^- state (fig. 4) could be resolved. The angular distribution for the 6.14 MeV state favours the highest spin value of the $J^\pi = (1^- - 4^+)$ possibilities given in ref. [27]), but even with $J = 4$ the forward-angle data are not well described by the calculations (fig. 4). The angular distribution of the unresolved doublet consisting of the 5.84 MeV 1^- and the 5.86 MeV 3^- states (fig. 4) is dominated by the $L = 3$ transition. No indication was found for the population of the 5.90 MeV 4^- state. The 6.36 MeV 4^+ state is weakly populated (fig. 4) as are the states at 6.61 MeV

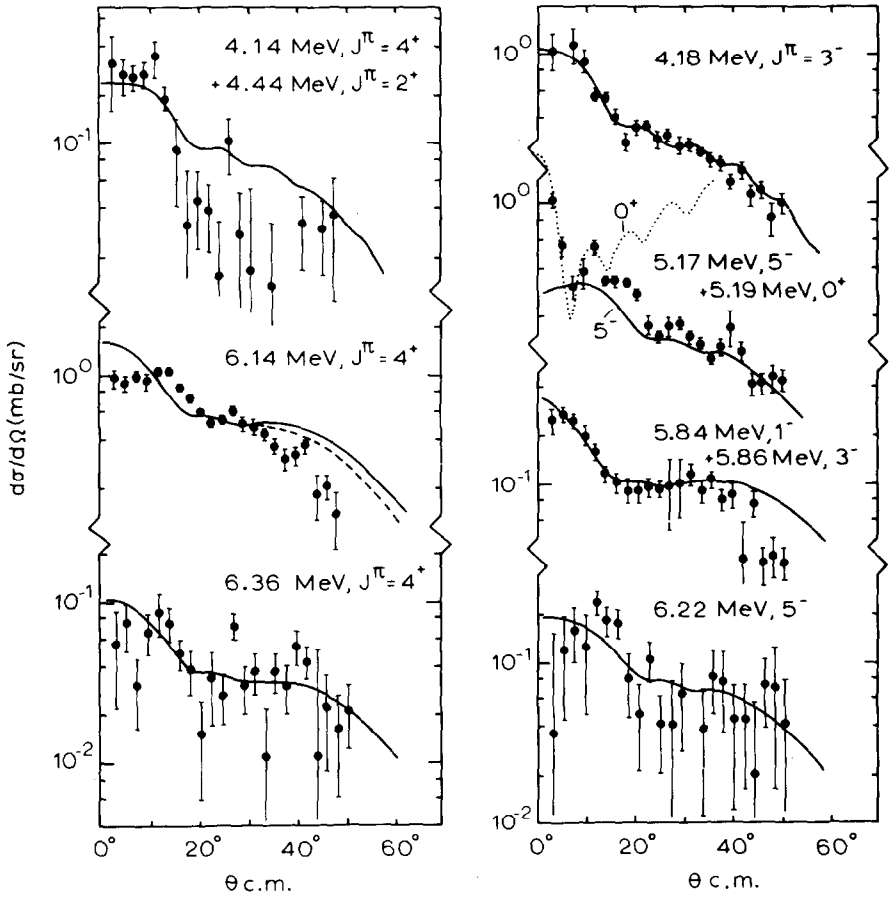

Fig. 4. Same as fig. 3, but for $J^\pi = 4^+$ states (left part) and for negative-parity states (right part). The curve for the $J^\pi = 2^+, 4^+$ doublet represents the sum of the two calculated angular distributions. For the $5^-, 0^+$ doublet the calculated angular distributions for the two components are given separately, while for the $1^-, 3^-$ doublet the sum is given.

($T = 1$) and 6.65 MeV for which only an upper limit to the cross section of 50 μb/sr was extracted.

The states above $E_x = 6.64$ MeV are unbound for α-decay. The angular distributions for the most strongly populated states in this region are given in fig. 5. The cross sections for other excited states in this region were found to be smaller than 100 μb/sr.

The relative strength of the transitions observed in the (^{16}O, ^{12}C) reaction is qualitatively the same as observed in the ^{32}S(^{6}Li, d)^{36}Ar reaction [28]) as measured at a single angle (see table 1). An exception may be the 4.33 MeV $(0)^+$ state which in the (^{6}Li, d) reaction is apparently much weaker populated than the ground state, while it is stronger than the ground state in the (^{16}O, ^{12}C) reaction.

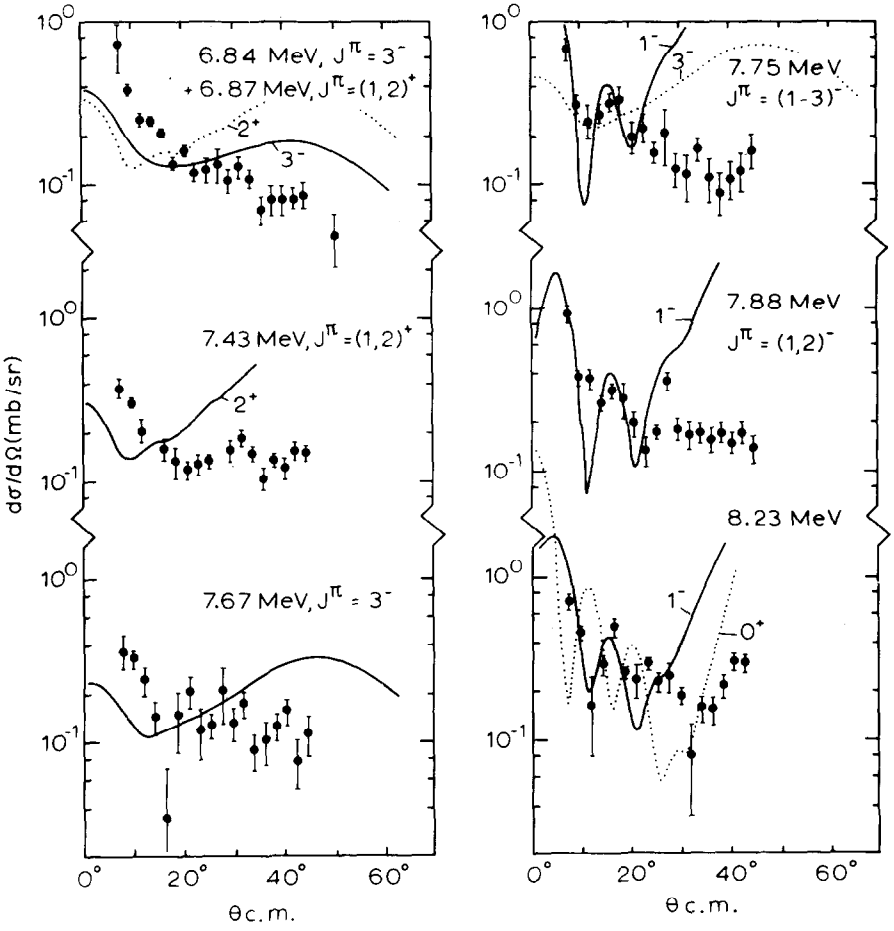

Fig. 5. Same as fig. 3, but for states which are unbound with respect to α-particle decay. The curves are DWBA calculations for the most probable J^π values, which include only the $q = 0$, $j_\alpha = 0$ form-factor components with $Q = 8$ (positive-parity) or $Q = 9$ (negative-parity) quanta in the relative motion of the $\alpha + {}^{32}S$ system.

3. DWBA analysis

3.1. FORMALISM

The calculations of four-nucleon transfer angular distributions presented in this section were performed in the framework of the exact finite-range distorted-wave Born approximation (DWBA) as discussed e.g. in ref. [29]). For later purposes a slightly more general expression [30]) is presented for the DWBA cross section of a stripping reaction A(a, b)B, with $a = b + \alpha$, $B = A + \alpha$ and α the transferred

TABLE 1

Comparison of cross sections for selected levels of ^{36}Ar, populated strongly in the ^{32}S(^{16}O, ^{12}C)^{36}Ar reaction at 45.5 MeV and in ^{32}S(^{6}Li, d)^{36}Ar at 32 MeV

E_x (MeV)	J^{π} [a]	$\left(\frac{d\sigma}{d\Omega}\right)^{max}$ (μb/sr) [b] (^{16}O, ^{12}C)	$\frac{d\sigma}{d\Omega}$ (μb/sr) [c] (^{6}Li, d)
0	0^+	710	46
1.97	2^+	540	11
4.18	3^-	1100	60
4.33	$[0^+]$	1070	9
4.95	2^+	3400	81
5.17	5^-	300	26 [d]
5.19	$[0^+]$	250	
5.84	1^-	260 [d]	41 [d]
5.86	3^-		
6.14	$[4^+]$	1050	60
6.84	3^-		
6.87	$(1, 2)^+$	400 [d]	25 [d]

[a]) The J^{π} values in brackets result from the present work.
[b]) For 0^+ states the cross section at the second maximum ($\theta_{c.m.} \approx 10°$) was taken.
[c]) Cross sections measured at $\theta_{lab} = 5°$, from ref. [28]).
[d]) Unresolved doublet.

cluster, which is valid in the absence of spin-orbit interactions:

$$\left(\frac{d\sigma}{d\Omega}\right)^{DWBA} = \frac{\mu_a \mu_b}{(2\pi\hbar^2)^2} \frac{k_b}{k_a} \frac{2J_B+1}{2J_A+1} \sum_{\substack{J_\alpha \bar{J}_\alpha \\ J\,M}} \left| \sum_{QL\bar{Q}\bar{L}} B^{QL,\bar{Q}\bar{L}}_{J_\alpha \bar{J}_\alpha J} I^{QL,\bar{Q}\bar{L}}_{JM} \right|^2 . \tag{1}$$

The factors in front of the sum contain the entrance and exit channel reduced masses μ, wave numbers k and the appropriate spin weight factors. The overlap integrals I describe the reaction dynamics through the distorted waves, the bound-state wave functions and the interaction potential connecting the initial and final channel. The bound-state wave functions are characterized by the angular momentum L and the number of oscillator quanta $Q = 2N + L$, where N is the number of radial nodes. The barred symbols are for the system $b + \alpha$ and the unbarred symbols for $A + \alpha$. The angular momenta L and $\bar{L}$ are coupled to a total angular momentum J with projection M. The factor B in the sum of eq. (1) contains the dependence on the nuclear structure and can be expressed as (introducing $\hat{j} = \sqrt{j+1}$)

$$B^{QL,\bar{Q}\bar{L}}_{J_\alpha \bar{J}_\alpha J} = i^J \sum_{q\gamma j_\alpha} \hat{j}_\alpha (-1)^{L+j_\alpha-J_\alpha} U(J_\alpha L \bar{J}_\alpha \bar{L}, j_\alpha J) A^*_{BA} A_{ab} . \tag{2}$$

Here U is a recoupling coefficient for three angular momenta. The spectroscopic amplitudes $A_{BA}[J_B J_A(q\gamma j_\alpha, QL)J_x]$ (and similarly A_{ab}) express the overlap of the nucleus B with different cluster states of the system $A+\alpha$, where the intrinsic structure of the α-clusters is indicated by the number of oscillator quanta q, a label γ and the spin j_α, which is coupled with the angular momentum of relative motion L to a total angular momentum J_x. The spectroscopic amplitudes are further discussed in sect. 4.

Eqs. (1) and (2) clearly show that in general it is not possible to factorize the expression for the reaction cross section in a structural and a dynamical part. Even if the usual assumption of 0s relative motion of the four nucleons in the cluster α is made, this factorization is only possible if not more than one combination of QL, $\bar{Q}\bar{L}$ contributes to the sum in eq. (1).

For a discussion of the calculated angular distributions it is useful to give the Legendre polynomial expansion of the cross section which can be obtained from a partial-wave expansion of the distorted waves (for particles a and b without spin)

$$\left(\frac{d\sigma}{d\Omega}\right)^{DWBA} \sim \sum_M \left|\sum_{L_b} \beta^M_{L_b} P^M_{L_b}(\cos\theta)\right|^2, \tag{3}$$

where L_b is the orbital angular momentum of the exit-channel partial waves and M has the same meaning as in eq. (1).

Special numerical techniques are required to evaluate the six-dimensional overlap integral I in eq. (1). In our analysis the calculations were performed with the computer code DWUCK5 [31]), which makes use of a plane-wave expansion technique introduced by Charlton [32]). Because this code has not yet been used much for heavy-ion reactions, we have checked its performance by reproducing several of the calculations of Peng *et al.* [17]) for the reaction ^{28}Si(^{16}O, ^{12}C)^{32}S at 42 MeV, both with DWUCK5 and with LOLA [33]). The deviations between calculations with the two codes were found to be less than 2%. The calculations with DWUCK5 were, however, more than ten times faster than those with LOLA.

In the formalism used by DWUCK5 it is not possible to include the proper Coulomb terms [34]) in the DWBA interaction potential. The influence of these terms has been extensively analyzed by Peng *et al.* [17]). They found about 20% changes in the absolute cross sections, while the shapes of the angular distributions did not change and the differences in relative cross sections were less than 10%.

For all calculations the post representation of the DWBA transition amplitudes was chosen. For the ground-state transition to ^{36}Ar the difference in absolute cross section between the prior and post representations is about 30%, which is at least partly caused by the neglect of the Coulomb interactions [34]).

3.2. THE BOUND-STATE WAVE FUNCTIONS

The bound-state wave functions were calculated in a potential well of Woods-Saxon shape, with the depth adjusted to reproduce the experimental separation energies of the α-particle. While this procedure may be the best approximation [35]) if only one (QL) component dominates the cluster expansion of the nucleus B (or a), it is not appropriate if more components contribute. Since the wave functions used for ^{36}Ar give rise to $Q = 8$ and 10 components, a natural extension of this procedure was used to determine the binding energies of each component. The two states of a certain spin with the largest $Q = 8$, respectively $Q = 10$ spectroscopic factors were chosen on the basis of the shell-model calculation. Then it is required that the sum of the binding energies of the two components, weighted with the corresponding spectroscopic factor, is equal to the separation energy of the α-particle for the chosen states. For other states of the same spin these binding energies were shifted (keeping their difference fixed) to reproduce again the experimental separation energy when weighted with the appropriate spectroscopic factors, with the restriction that they cannot become unbound. One should keep in mind that this procedure is an approximation, because one should consider the mixing of cluster states in that part of the wave function of the nucleus, that is probed in the reaction, which takes place predominantly at the nuclear surface. The shell-model spectroscopic amplitudes, however, are a good measure of the mixing only in the nuclear interior. For the geometry of the Woods-Saxon well a radius $R = 1.25\ (A_c+4)^{\frac{1}{3}}$ fm and a diffuseness $a = 0.65$ fm were taken, where A_c is the atomic number of the core to which the α-particle is bound. With this choice we follow the arguments of ref. [36]). The same potential was also used for the DWBA interaction potential.

3.3. OPTICAL POTENTIALS

From an extensive search for optical potentials to describe the ^{32}S(^{16}O, ^{12}C)^{36}Ar reaction data it was found that surface-transparent potentials were needed in order to describe the strongly oscillating and forward rising angular distributions especially for the ground state and the first 2^+ state. Surface-transparent potentials are characterized by an imaginary part with smaller radius and diffuseness parameters than used for the real part. As a starting point the potential set used in ref. [17]) was chosen (pot. I of table 2). This set was originally derived from ^{16}O elastic scattering and transfer reactions on ^{64}Ni [ref. [37])]. It was found that this potential produces a good description of the elastic scattering data, not only for ^{16}O + ^{32}S [ref. [26])] and for ^{16}O + ^{28}Si [ref. [10])] ($\theta_{c.m.} < 90°$), but also for the system ^{12}C + ^{40}Ca [ref. [38])] at angles $\theta_{c.m.} < 90°$, while the scattering of ^{12}C from ^{28}Si [ref. [9])] was reasonably well reproduced.

Angular distributions calculated with pot. I for the 0_1^+ and 2_1^+ states in ^{36}Ar are

TABLE 2

Optical potential sets used in the DWBA analysis of the $^{32}S(^{16}O, ^{12}C)^{36}Ar$ reaction at $E_{lab} = 45.5$ MeV

	System	V (MeV)	r_V [a]) (fm)	a_V (fm)	W (MeV)	r_W [a]) (fm)	a_W (fm)	r_C [a]) (fm)	Ref.
pot. I [b])	$^{16}O+^{32}S$ $^{12}C+^{36}Ar$	35	1.307	0.493	20	1.242	0.204	1.30	[37])
pot. II	$^{12}C+^{36}Ar$	29	1.318	0.457	9.2	1.211	0.190	1.30	[9])
bound	$^{32}S+\alpha$	[c])							
states	$^{12}C+\alpha$		1.25	0.65	–	–	–	1.30	–

[a]) The radii of the Woods-Saxon and Coulomb potentials are given by $R = r(A_1^{1/3} + A_2^{1/3})$ for the entrance and exit channels and by $R = r(A_1 + A_2)^{1/3}$ for the bound states; A_1 and A_2 are the mass numbers of the interacting nuclei.

[b]) In the final analysis pot. I was used for both entrance and exit channel.

[c]) The depth of the bound-state potentials was adjusted to reproduce the experimental separation energies.

given in fig. 6 (with $Q = 8$ for the bound-state wave functions). The agreement with the measured angular distributions is reasonably good, although the period of the oscillations could be somewhat larger, especially for the 2_1^+ state.

It is noteworthy that fits to elastic scattering tend to give a smaller value for the depth W of the imaginary potential than the $W = 20$ MeV of pot. I, which is not in accord with the reaction data. The effect of changing W of pot. I to 7 MeV is illustrated in fig. 6 by the dashed curves, which show an enhancement of the angular distributions at angles $\theta_{c.m.} > 20°$. These deviations can be understood from fig. 7, in which the coefficients of the Legendre polynomial expansion $|\beta_L|$ (eq. (3)) of the calculated ground-state angular distributions are plotted as a function of the partial-wave angular momentum L. Especially the region $L = 14$–20 is of interest. The solid curve corresponding to pot. I is characterized by a very narrow peak around $L = 21$ (the grazing angular momentum in both the entrance and the exit channel is $L_{gr} = 20$). The partial waves with $L \leqq 16$ hardly contribute to the cross section. This strong localization in L-space is typical for surface transparency. The dashed curve for the shallow imaginary potential, on the other hand, shows wild fluctuations as a function of L up to $L = 18$. This observation suggests that the nuclear interior is too transparent with the shallow imaginary potential. To make this more clear we have added to this potential an extra absorption term of depth $W' = 20$ MeV with a small radius parameter $r'_w = 1.0$ fm (and $a' = 0.2$ fm) corresponding to the critical distance for fusion. The disappearance of fluctuations in the dot-dashed curves in fig. 7 shows that the nuclear interaction at relatively small distances still plays an important role. The more regular behaviour of the lower-L partial waves effected by the extra absorption gives a considerable improvement (see fig. 6).

In the calculations so far the same potential was used in entrance and exit

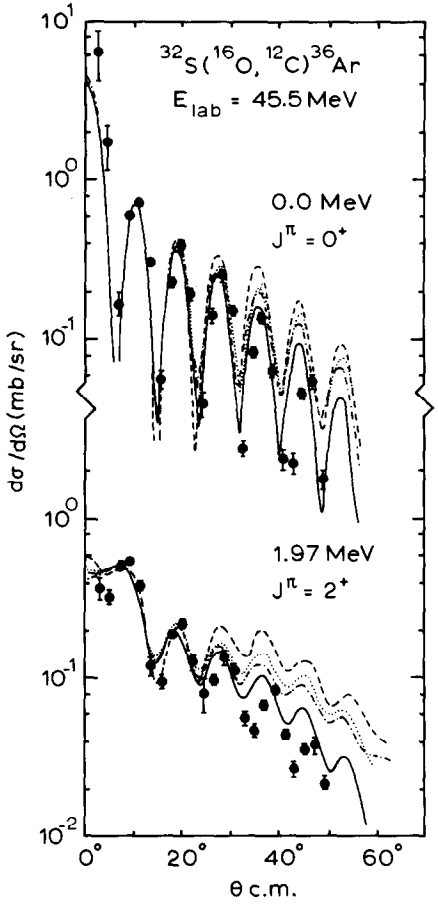

Fig. 6. Angular distributions for the $^{32}S(^{16}O, ^{12}C)^{36}Ar$ reaction to the ground state and first excited 2^+ state of ^{36}Ar. The curves are DWBA results calculated with different optical potentials, which are discussed in the text.

channel. Of the specific ^{12}C potentials found in the literature, the pot. II (table 2) obtained by Cheng *et al.*[9]) from a fit to $^{12}C+^{28}Si$ elastic scattering gave the best results also for the transfer angular distributions. This potential is fairly equivalent to pot. I, the main difference being a smaller imaginary radius parameter and depth. The results for the α-transfer to the ground state and 2_1^+ state of ^{36}Ar are not as good as when pot. I is also used in the exit channel (dotted curves in fig. 6). The dotted curve in fig. 7 shows that the dominant peak in the partial-wave expansion is broader with the combination of pot. I and II. For further calculations it was therefore decided to use pot. I in both entrance and exit channel.

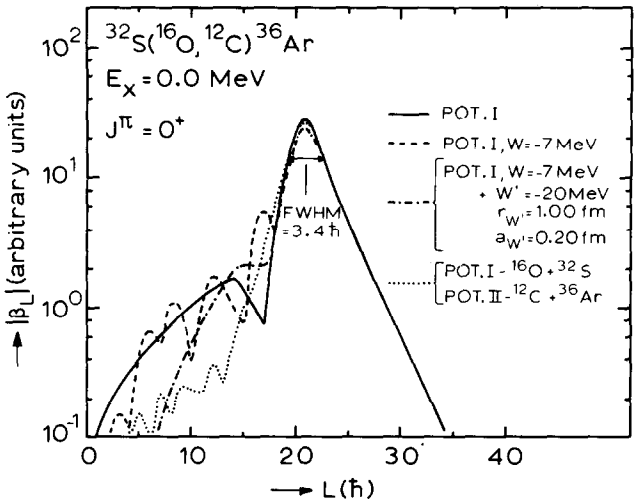

Fig. 7. Partial wave expansion of the DWBA transition amplitude for the ground-state angular distribution (see eq. (3)). The curves correspond to the calculated angular distributions of fig. 6.

3.4. SHELL-MODEL CALCULATIONS

For the calculation of spectroscopic amplitudes two sets of wave functions were used for the states of ^{36}Ar and the ground state of ^{32}S. The first set was obtained with the empirical interaction of Chung and Wildenthal [39]) in the full sd-shell model space (referred to as TH1). Only the positive-parity states can be calculated within this model. The excitation energies of the first 2^+ state and the $0^+ - 2^+ - 4^+$ triplet at $E_x \approx 4.4$ MeV in ^{36}Ar are well reproduced but this model fails to reproduce the energies of higher excited states. The second set of wave functions was obtained by Van der Poel *et al.* [40]) in a $(sd)^{8-n}(fp)^n$ model space with a SDI interaction (TH2). In these calculations the $0d_{\frac{3}{2}}$ orbit was assumed to be fully occupied (^{28}Si as an inert core) and $n = 1$ or 2 nucleons were allowed to occupy the $0f_{\frac{7}{2}}$ or $1p_{\frac{3}{2}}$ orbits for the negative- and positive-parity states, respectively. Details of these calculations can be found in ref. [40]). For ^{36}Ar a one-to-one correspondence can be made between the experimentally known levels and those calculated below $E_x = 6.5$ MeV, although the average deviation of about 420 keV between the experimental and calculated excitation energies is not sufficiently small to make this correspondence unambiguous. Of special interest is the occurence in the calculated level scheme of two 0^+ states at 4.8 and 5.0 MeV, which may be identified with the states at $E_x = 4.33$ MeV and 5.19 MeV, supporting our conclusions about the spins of these states from the apparent $L = 0$ character of the angular distributions for these states (see figs. 3 and 4).

Wave functions for the ground states of ^{16}O and ^{12}C and the first excited state

of ^{12}C were obtained from the work of Van Hees and Glaudemans[41]). The spectroscopic factors for the transitions $^{16}O \rightarrow {}^{12}C(g.s.)+\alpha$ ($S = 0.25$) and $^{16}O \rightarrow {}^{12}C(2_1^+)+\alpha$ ($S = 1.30$) calculated with these wave functions are in perfect agreement with earlier calculations[42]).

3.5. DISCUSSION OF DWBA RESULTS FOR BOUND STATES

In a first analysis the transferred four nucleons were assumed to be in their ground state of internal motion ($q = 0$, $j_\alpha = 0$). The quantum numbers of the bound-state wave functions are then determined by

$$Q = 2N + L = \sum_{i=1}^{4} 2n_i + l_i, \tag{4}$$

where n_i, l_i are the quantum numbers of the shell-model orbits occupied by the individual nucleons. For $^{16}O \rightarrow {}^{12}C+\alpha$ one has $Q = 4$, whereas for $^{32}S+\alpha \rightarrow {}^{36}Ar$ one gets $Q = 9$ for the negative-parity states and $Q = 8$ or 10 for the positive-parity states. The spectroscopic amplitudes entering the DWBA calculations were obtained with the formalism described in sect. 4.

To facilitate the comparison with experiment the calculated angular distributions (eqs. (1), (2)) were normalized as

$$\left(\frac{d\sigma}{d\Omega}\right)^{exp} = N\varepsilon\left(\frac{d\sigma}{d\Omega}\right)^{DWBA}, \tag{5}$$

where N is an overall normalization factor, determined from the ground-state transition (for which $\varepsilon \equiv 1$) and the enhancement factor ε is a measure of the agreement between experimental and calculated cross sections.

Some examples of angular distributions calculated with spectroscopic amplitudes obtained with the TH1 and TH2 models (dotted and solid curves, respectively) are given in fig. 8. For other transitions one is referred to figs. 3–5. Although the curves in these figures were obtained with the complete calculations of sect. 4, the shapes of the angular distributions differ only marginally from those obtained if only the ground-state cluster is considered. A first remark about fig. 8 concerns the differences between the TH1 and TH2 curves. The longer-ranged radial tail of the $Q = 10$ bound-state wave functions, which contribute to the TH2 calculations for positive-parity states, causes only a slight rise of the angular distributions at larger angles. The relative contributions of the $Q = 8$ and $Q = 10$ components are given in table 3 as spectroscopic amplitudes.

The calculated shapes of the angular distributions are in good agreement with the data for the transitions to the ground state and the first 2^+ state at 1.97 MeV (fig. 8) and for all bound negative-parity states (fig. 4). The scaling factors ε (eq.

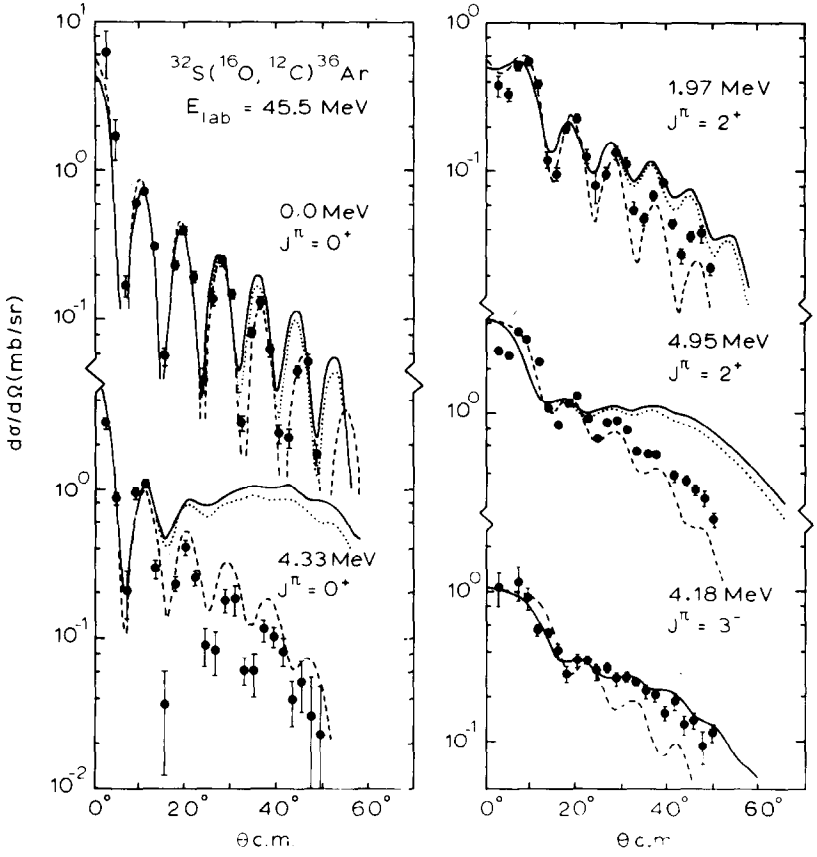

Fig. 8. Angular distributions for some strong transitions in the reaction $^{32}S(^{16}O, ^{12}C)^{36}Ar$. The curves are DWBA calculations with different bound-state wave functions, which are discussed in the text.

(5)) corresponding to these curves are given in table 3. They indicate that also the absolute cross sections (relative to the ground state) are correctly reproduced for these states. The value of ε for the first 2^+ state is much better when the wave functions of the TH2 model ($\varepsilon = 0.9$) are used than with the Chung-Wildenthal wave functions ($\varepsilon = 2.2$). This illustrates the importance of fp-shell admixtures even in the lowest excited states of ^{36}Ar. The description of the $(2^+, 4^+)$ doublet at 4.4 MeV (fig. 4) is acceptable, taking into account the experimental uncertainties and the small theoretical spectroscopic amplitudes for these states.

The two 0^+ states at 4.33 MeV (fig. 8) and 5.19 MeV (fig. 4) are, however, not well described nor are the strong transitions to the 4.95 MeV 2^+ (fig. 8) and the 6.14 MeV 4^+ (fig. 4) states. These calculated angular distributions show a strong tendency to rise at larger angles. While for the 0^+ states the shape for $\theta_{c.m.} < 15°$ is still correct, the 2^+ and 4^+ state angular distributions deviate also in the small-

TABLE 3

Shell-model spectroscopic amplitudes for $\alpha(q = 0,\ j_\alpha = 0)$ transfer and comparison of DWBA calculations with experimental cross sections

E_x (MeV)	J^π [a]	$A_{TH1}(\times 10^{-4})$ [b]	$A_{TH2}(\times 10^{-4})$ [c]		ε_{TH1} [d]	ε_{TH2} [d]
		$Q = 8$	$Q = 8$ or $Q = 9$	$Q = 10$		
0	0^+	2640	−1210	434	$N = 42$	$N = 73$
1.97	2^+	704	− 520	182	2.2	0.9
4.18	3^-		−911			1.0
4.33	$[0^+]$	−142	− 91	−1020	3.10^3	28
4.44	$2^+(^{12}C^*)$	11420 [e]			3.4	4.5
4.41	4^+	−287	237	− 73 [f]	< 7	< 3
4.44	2^+	− 91	− 30	− 29		
4.95	2_3^+	−209	− 54	63	(270)	450
	2_4^+		80	957		(4.8)
5.17	5^-		986			0.6
5.19	$[0^+]$	74	33	263	(10^4)	500
5.84	1^-		602	[f]		1.0
5.86	3^-		−585			
6.14	$[4_2^+]$	−124	74	− 7	(270)	340
	$[4_3^+]$	345	− 13	−700	(35)	2.6
6.22	5^-		359			2.3
6.36	4_3^+	345	− 13	−700	(2.4)	0.24
	4_4^+	− 124	74	− 7	(19)	23

[a]) Spin-parity values in brackets are probable assignments from the present work. Lower-right indices indicate the sequence number of the J^π state in the calculations.

[b]) Spectroscopic amplitudes for $^{32}S + \alpha \rightarrow {}^{36}Ar$ calculated from wave functions obtained in the full sd-model space (TH1) for which the relative motion of the $\alpha(q = 0, j_\alpha = 0^+)$ cluster with respect to the ^{32}S core contains $Q = 8$ oscillator quanta.

[c]) Spectroscopic amplitudes calculated in a $(sd)^{8-n}(fp)^n$ model space with $n \leqq 2$ (TH2 model). Amplitudes are given for the $Q = 8$ and 10 components of relative motion for the positive-parity states. The two components interfere constructively in the DWBA calculation if the amplitudes are of opposite sign. For the negative-parity states $Q = 9$.

[d]) Enhancement factors for the two theoretical models TH1 and TH2 (see eq. (5)). For the ground-state transition one has $\varepsilon \equiv 1$ and in the first entry of the ε-columns the overall normalization factor N is given. The $^{16}O \rightarrow {}^{12}C(g.s.) + \alpha$ spectroscopic amplitude used in both calculations equals $A = 0.501$. Values of ε for states of which the excitation energy is calculated too far from the experimental values to make a reliable identification have been put in parentheses.

[e]) State of ^{12}C; the $^{16}O \rightarrow {}^{12}C + \alpha$ spectroscopic amplitude is given.

[f]) Unresolved doublet.

angle region. Also the very large enhancement factors (ε_{TH2} = 30–550, see table 3) indicate that the description of these transitions is incorrect. The enhancement factor for the 4.95 MeV 2^+ state can be improved somewhat if it is identified with the fourth 2^+ state found in the calculated level scheme ($\varepsilon = 5$). The excitation energy of this state is, however, calculated 1.1 MeV too high. Similarly, the third

4^+ state gives a better enhancement factor for the 6.14 MeV state ($\varepsilon = 2.6$), but then the assignment of the second 4^+ to the 6.36 MeV state (fig. 4) makes ε for this state too large, which transition was with the third 4^+ wave function in reasonable agreement with the data (see table 3). In any case, these ambiguities do not affect the conlusions about the calculated angular distribution shapes, which first ask for an explanation. The present theoretical model can certainly not account for the total strength observed experimentally for these 0^+, 2^+ and 4^+ states.

In a further investigation of the noted discrepancies, the emphasis was on the most pronounced cases, the 4.95 MeV 2^+ state and especially the 4.33 MeV 0^+ state. For the transition to the latter state the partial wave distribution of the DWBA matrix elements $|\beta_L|$ (eq. (3)) is given in fig. 9, together with the reflection functions $|\eta_L|$ [see e.g. ref. [1])] for the elastic scattering in entrance and exit channels. The tail in $|\beta_L|$ for $L < 16$ hardly contributes to the cross section because of the rapidly varying phase of the β_L in this region. The angular distribution is completely determined by the peak around $L = 19$, which for the 4.33 MeV transition clearly is much broader than for the ground-state transition (compare fig. 7). The connection of this feature with the large angular momentum mismatch of $\Delta L \approx 4$ between entrance and exit channel may be evident from a comparison with the corresponding reflection functions. While the top of the $|\beta_L|$ peak still corresponds to about the grazing angular momentum in the entrance channel $L = 20$, it is seen that the L-values between $L = 16$ (the grazing angular momentum

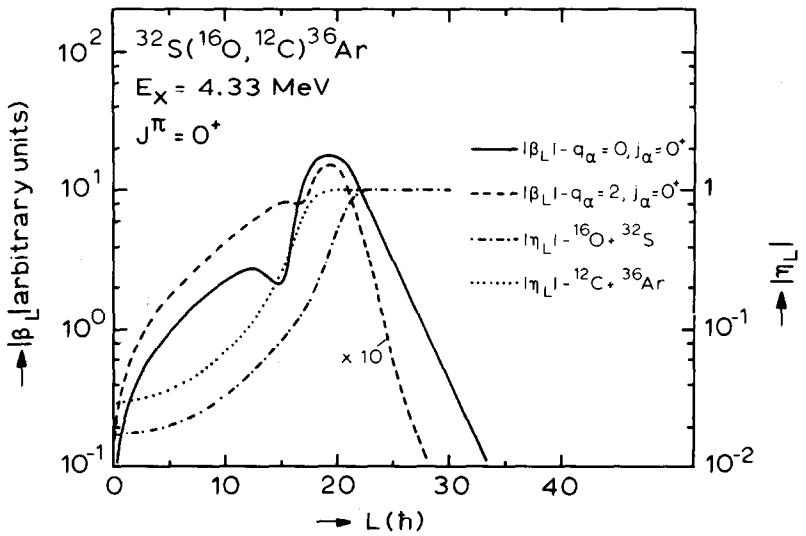

Fig. 9. Partial-wave decomposition (see eq. (3)) of angular distributions for the transition to the $E_x = 4.33$ MeV $J^\pi = 0^+$ state. The solid and dashed curves are expansion coefficients corresponding to the calculated angular distributions of fig. 8 for this transition. The dot-dashed and dotted curves give the elastic scattering reflection coefficients $|\eta_L|$ for the entrance and exit channel, respectively, of the transition to this second 0^+ state.

in the exit channel) and $L = 18$ also contribute considerably due to the incomplete absorption of these partial waves in the entrance channel. Therefore we tried to improve the 4.33 MeV 0^+ fit by varying the absorptive properties of the optical potentials. No reasonable description could, however, be found with any potential of the volume Woods-Saxon type. Some success was obtained with an L-dependent absorption of the type introduced by Chatwin *et al.*[43]), but only if the absorption for the entrance-channel grazing partial waves was made so weak that it gave rise to an orbiting resonance, which produced unacceptably large oscillations in the elastic scattering angular distribution.

By changing the radial shape of the bound-state wave functions the shape of the angular distributions can in principle be described. The dashed curves in fig. 8 for the 4.33 and 4.95 MeV transitions were calculated with the four nucleons transferred as a cluster with $q = 2$ quanta in the internal motion. This causes the binding energies with respect to the ^{32}S and ^{12}C cores to be quite large (≈ 20 MeV and 25 MeV, respectively) and correspondingly the radial tails of the wave functions fall off much steeper with increasing radius than for the $q = 0$ cluster. It is seen from fig. 8 that the dashed curves approach the experimental shape of the angular distributions quite well. The dashed $|\beta_L|$ curve in fig. 9 shows that the excited-cluster wave functions affect especially the higher partial waves ($L > 20$), which are rather insensitive to the optical potentials. However, the much smaller intrinsic DWBA cross sections for such form factors in comparison with $q = 0$ transfer ($\sigma_{q=0}/\sigma_{q=2} \approx 30$ or 100 for the 4.33 and 4.95 MeV states, respectively) require very large spectroscopic amplitudes to reproduce the absolute cross sections. We have calculated these amplitudes on a formal shell-model basis, thereby stimulated by the work of Kurath and Towner[30]) who showed that the $q = 0$ component in the cluster expansion of $^{16}O \rightarrow {}^{12}C + \alpha$ represents only 8% of the total strength. The results of these calculations are discussed in sect. 4.

The large normalization factors $N_{TH1} = 42$ and $N_{TH2} = 73$ (see table 3), needed to reproduce the magnitude of the cross section for the ground state, are a well known problem in transfer reactions with heavy ions. This problem has been discussed e.g. by Fliessbach[44,45]), who ascribes it to a misrepresentation of the antisymmetrization of the transferred nucleons in the conventional method of calculating α-particle spectroscopic factors. For sd-shell nuclei Fliessbach estimates the ground-state spectroscopic factors to be a factor of 4 ($^{20}Ne \leftrightarrow {}^{16}O + \alpha$) [ref.[45])] to 10 ($^{40}Ca \leftrightarrow {}^{36}Ar + \alpha$) [ref.[44])] larger than the conventional values.

3.6. THE ^{12}C(4.44 MeV) EJECTILE EXCITATION

In the angular distribution for the 4.44 MeV 2^+ state in ^{12}C (fig. 3) the $L = 2$ character can be clearly recognized. The agreement of the calculated curve with the experimental results is not very good, although the tendency to rise at $\theta_{c.m.} > 20°$ can also be observed in the data. Most astonishing, however, is that the

experimental cross section (relative to the ground-state transition) is about a factor of 4 larger than predicted by both theoretical models. For the ^{24}Mg(^{16}O, ^{12}C*)^{28}Si reaction [17,36]) this ratio was found to be very well in accord with the theoretical prediction [calculated with the same optical potentials in ref. [17])]. Population of the 4.44 MeV ^{12}C state was not observed in the reaction ^{28}Si(^{16}O, ^{12}C*)^{32}S [refs. [17,18])], where it is, however, obscured by other transitions. By Peng *et al.* [17]) the different population of the ^{12}C(4.44 MeV) state in these reactions was explained by the Q-value dependence of the cross sections, which is influenced by the bound-state wave function of the projectile. The negative ground-state Q-value for the reaction on ^{28}Si($Q_{g.s.} = -0.21$ MeV) makes this transition unfavourable in comparison with the reaction on ^{24}Mg($Q_{g.s.} = +2.82$ MeV). Therefore, one would expect the ejectile excitation in the ^{32}S(^{16}O, ^{12}C*)^{36}Ar reaction to be weak, because for this reaction $Q_{g.s.} = -0.52$ MeV. The fact that it is rather strong may point to a two-step mechanism for the excitation of the ^{12}C(4.44 MeV) state.

3.7. UNBOUND STATES

Angular distributions for states in ^{36}Ar with $E_x > 6.6$ MeV are given in fig. 5. The fact that these states are unbound for α-decay complicates the DWBA analysis. If, however, the width of the resonance is sufficiently small, the cross section may be approximated by the normal stripping cross section on the resonance [46]). The prior representation was used to make sure that the radial integrals converge [47]). The results of the calculations are shown in fig. 5. They deviate strongly from the experimental angular distributions. Nevertheless some conclusions can be drawn from these results. All calculated curves show a strong rise at larger angles ($\theta_{c.m.} > 20°$) which is apparently Q-value dependent. This tendency can also be noted in some of the experimental angular distributions (for $E_x = 7.43$, 7.75 and 8.23 MeV), albeit at much larger angles. The qualitative similarity of these features with those observed for some of the bound positive-parity states, suggests that the origin of the discrepancies can be found in the reaction dynamics, connected with a large angular momentum mismatch, as will be discussed in sect. 5.

4. Calculations with excited cluster configurations

The statement that the (^{16}O, ^{12}C) reaction is a good "α-transfer" reaction relies on the assumption that the four nucleons are transferred as a cluster with minimum energy in the internal degrees of freedom. Extensive calculations to estimate the contribution of clusters with other intrinsic structures have only been presented in a limited number of cases. The calculations of Bock and Yoshida [48]) for three- and four-nucleon transfer with p-shell and lower sd-shell targets and projectiles do show significant differences when all terms in the cluster expansion

are taken into account. Therefore such calculations for the (^{16}O, ^{12}C) reaction on ^{32}S were performed.

The DWBA formalism was presented in sect. 3 in the general form given by Kurath and Towner [30]. The spectroscopic amplitudes $A_{BA}[J_B J_A(q\gamma j_\alpha, QL)J_\alpha]$ and $A_{ab}[J_a J_b(q\gamma j_\alpha, \bar{Q}\bar{L})\bar{J}_\alpha]$ entering these equations can be expressed [30]) as

$$A_{BA} = \left(\frac{B}{B-4}\right)^{\frac{1}{2}Q} \sum_{\Gamma} J_B^{-1} \langle \psi^{J_B} || \chi^{J_\alpha \Gamma^\dagger} || \psi^{J_A} \rangle \, G(J_\alpha \Gamma, q\gamma j_\alpha, QL), \tag{6}$$

where the first factor stems from a transformation of the spatial coordinates of the cluster α. The double-barred bracket is the reduced matrix element of a four-nucleon creation operator $\chi^\dagger$, with total angular momentum J_α and a label Γ to specify the shell-model basis states for the four nucleons. The wave functions ψ^{J_B} and ψ^{J_A} for the parent and daughter nuclei can be expanded in a shell-model basis and the reduced matrix elements can be evaluated with standard shell-model techniques [49,50]). The G-factor or structure factor in eq. (6) expresses the overlap of the shell-model wave function corresponding to the operator $\chi^{J_\alpha \Gamma^\dagger}$ with a wave function representing the cluster in terms of relative coordinates between nucleons and pairs of nucleons. The former representation can be transformed into the latter by first writing the (antisymmetric) four-particle wave functions in terms of products of two-particle wave functions. After recoupling from the *jj* to the *ls* coupling scheme, the spatial coordinate transformations can be performed by three consecutive Talmi-Moshinsky transformations with some additional angular momentum recouplings. After integration the complete expression for the G-factor of eq. (6) becomes

$$\begin{aligned}
G(J_\alpha \Gamma, q\gamma j_\alpha, QL) = {} & \sum_{\substack{\Gamma_1 \Gamma_2 \\ \gamma_1\gamma_2\gamma_3\gamma_4}} \hat{J}_\alpha^{-1} \left(\tfrac{4}{2}\right)^{-\frac{1}{2}} \langle J_\alpha \Gamma || [(\gamma_1\gamma_2)\Gamma_1 || (\gamma_3\gamma_4)\Gamma_2 \rangle \\
& \times \frac{2\delta_{\Gamma_1,\mathrm{odd}}\delta_{\Gamma_2,\mathrm{odd}}}{\sqrt{1+\delta_{\gamma_1\gamma_2}}\sqrt{1+\delta_{\gamma_3\gamma_4}}} (-1)^{S_\alpha+\lambda_\alpha+\lambda_r-j_2} \hat{j}_1\hat{j}_2\hat{j}_3\hat{j}_4\hat{J}_1\hat{J}_2\hat{S}_1\hat{S}_2\hat{S}_\alpha\hat{\lambda}_\alpha\hat{l}_\alpha\hat{j}_\alpha \\
& \times \sum_{\substack{L_1 L_2 L_\alpha \\ N_1\Lambda_1 N_2\Lambda_2\Lambda_\alpha}} \hat{L}_1^2\hat{L}_2^2\hat{L}_\alpha^2\hat{\Lambda}_\alpha^2 \begin{Bmatrix} l_1 & \frac{1}{2} & j_1 \\ l_2 & \frac{1}{2} & j_2 \\ L_1 & S_1 & J_1 \end{Bmatrix} \begin{Bmatrix} l_3 & \frac{1}{2} & j_3 \\ l_4 & \frac{1}{2} & j_4 \\ L_2 & S_2 & J_2 \end{Bmatrix} \begin{Bmatrix} L_1 & S_1 & J_1 \\ L_2 & S_2 & J_2 \\ L_\alpha & S_\alpha & J_\alpha \end{Bmatrix} \\
& \times \langle \nu_1\lambda_1 N_1\Lambda_1; L_1 | n_1 l_1 n_2 l_2; L_1 \rangle \langle \nu_2\lambda_2 N_2\Lambda_2; L_2 | n_3 l_3 n_4 l_4; L_2 \rangle \\
& \times \begin{Bmatrix} \lambda_1 & \Lambda_1 & L_1 \\ \lambda_2 & \Lambda_2 & L_2 \\ \lambda_\alpha & \Lambda_\alpha & L_\alpha \end{Bmatrix} \langle \nu_r\lambda_r NL; \Lambda_\alpha | N_1\Lambda_1 N_2\Lambda_2; \Lambda_\alpha \rangle \begin{Bmatrix} \lambda_\alpha & \lambda_r & l_\alpha \\ L & L_\alpha & \Lambda_\alpha \end{Bmatrix} \begin{Bmatrix} L & l_\alpha & L_\alpha \\ S_\alpha & J_\alpha & j_\alpha \end{Bmatrix}.
\end{aligned} \tag{7}$$

In this equation the order of the Wigner 9J and 6J symbols (curly brackets) and Talmi-Moshinsky brackets reflects the order in which the consecutive transformations have been performed. The double-barred bracket is a reduced matrix element of the same type as those appearing in eq. (6) and can be regarded as a two-particle coefficient of fractional parentage operating in different orbits. The γ_i represent the quantum numbers $(nlj)_i$ of the orbits occupied by the nucleons and Γ_i the quantum numbers $(J\,T)_i$ of the pairs. The factor with the δ-functions results from the antisymmetry of the nucleon pairs, $\bar{\Gamma}_i = \lambda_i + S_i + T_i$. The condition of conservation of the number of oscillator quanta for the Talmi-Moskinsky brackets imposes the following restriction on the number of quanta q in the intrinsic structure of the cluster:

$$q + Q = \sum_{i=1}^{4} (2n_i + l_i) = 2\nu_1 + \lambda_1 + 2\nu_2 + \lambda_2 + 2\nu_r + \lambda_r + 2N + L. \tag{8}$$

The spectroscopic amplitudes for target and projectile A_{BA} and A_{ab} can now be substituted in eq. (2) (sect. 3) and the sum over all intrinsic quantum numbers γ of the cluster can be performed except for the sum over q and j_α because different values of q, j_α imply different values of $\bar{Q}$, $\bar{L}$ and/or Q, L. At this point it should be remarked that in the derivation of eqs. (1), (2) the assumption has been made that the intrinsic cluster wave functions for projectile and target are orthonormal which implies the assumption of equal oscillator constants for the nuclei a and B.

Calculations were performed with both sets of wave functions TH1 and TH2, discussed in subsect. 3.2. Some numerical results are given in table 4 for the transitions to the two 0^+ states at 0 and 4.33 MeV and the two 2^+ states at 1.97 and 4.44 MeV in ^{36}Ar. The quantity

$$P(qj_\alpha, \bar{Q}\bar{L}, QL) = \sum_{\gamma} A^{*}_{\mathrm{BA}}[J_{\mathrm{B}} J_{\mathrm{A}} (q\gamma j_\alpha, QL) J_\alpha] A_{\mathrm{ab}}[J_{\mathrm{a}} J_{\mathrm{b}} (q\gamma j_\alpha, \bar{Q}\bar{L}) \bar{J}_\alpha] \tag{9}$$

is given for all possible combinations of quantum numbers $(qj_\alpha, \bar{Q}\bar{L}, QL)$. The component with $(q = 0, j_\alpha = 0)$ has in none of these cases the largest amplitude. On the other hand, the amplitudes for excited configurations are in general not more than two times as large. Only if the $(q = 0, j_\alpha = 0)$ component is very small as in the case of the 4.44 MeV 2^+ state, other configurations can become dominant as will become clear in the DWBA calculations.

Following ref.[48]) the excited clusters were bound in a potential well with a fixed depth obtained for the corresponding $(q = 0, j_\alpha = 0)$ cluster with the procedure described in sect. 3. The resulting binding energies are about 9, 18, 27 and 36 MeV larger for the $q = 1$–4 clusters, respectively, than for the corresponding $q = 0$ cluster, depending only slightly on the spin (j_α) and orbital angular momentum (L). In our version of the computer code DWUCK5 up to eight different form factor

TABLE 4

Spectroscopic amplitude products for all terms in the cluster expansion of the four nucleons transferred in the $^{32}S(^{16}O, ^{12}C)^{36}Ar$ reaction, for some selected final states

qj_α [a]	$\bar{Q}\bar{L}$ [b]	QL [c]	P_8 [d] ($\times 10^{-4}$)	P_{10} [e] ($\times 10^{-4}$)	P_8 [d] ($\times 10^{-4}$)	P_{10} [e] ($\times 10^{-4}$)
			$E_x = 0$ MeV, $J^\pi = 0^+$		$E_x = 4.33$ MeV, $J^\pi = 0^+$	
00	40	80	−607	217	− 46	−511
11	31	71	−393	−4	− 63	15
20	20	60	−414	154	− 89	−452
22	22	62	−517	66	− 13	− 60
31	11	51	−524	33	− 96	−120
40	00	40	−720	228	−103	−781
			$E_x = 1.97$ MeV, $J^\pi = 2^+$		$E_x = 4.44$ MeV, $J^\pi = 2^+$	
00	40	82	−260	91	− 15	− 14
11	31	71	− 91	−5	− 12	3
11	31	73	−194	8	71	− 13
20	20	62	−208	67	87	− 23
22	22	60	−188	39	34	− 9
22	22	62	− 14	−4	−120	15
22	22	64	−182	8	12	4
31	11	51	−139	6	37	1
31	11	53	−289	22	164	− 16
40	00	42	−331	94	148	− 43

[a]) The number of oscillator quanta q in the intrinsic structure of the cluster and the spin j_α of the cluster; the parity $\pi = (-1)^q$.

[b]) Quantum numbers of the relative motion of the cluster with respect to the ^{12}C core; $\bar{Q}$ is the number of oscillator quanta and $\bar{L}$ is the orbital angular momentum.

[c]) Quantum numbers of the relative motion of the cluster with respect to the ^{32}S core.

[d]) Product of spectroscopic amplitudes for target and projectile, summed over all intrinsic quantum numbers of the cluster except q and j_α (see eq. (9)). The amplitudes were calculated with wave functions from the TH2 model discussed in subsect. 3.2. The total number of quanta for the components in this column is $q+Q = 8$. Components with equal sign interfere predominantly constructively in the DWBA transition matrix.

[e]) See [d]). The total number of quanta for these components is $q+Q = 10$. All quantum numbers given in the first columns pertain to these components, except for Q which is 2 units larger. Components with $q+Q = 8$ and 10 interfere constructively if they have opposite signs.

components could be handled simultaneously. This was thought to be sufficient for the present purposes and for each transition the eight strongest components were selected.

The resulting angular distributions are given in figs. 3–5. From a comparison with fig. 8 it can be seen that the shapes of the angular distributions do not differ much from those calculated with only the ($q = 0$, $j_\alpha = 0$) components. The cross sections tend to be somewhat smaller at larger angles. A comparison of absolute

TABLE 5

Results of DWBA calculations for transfer of four-nucleon clusters in excited configurations

E_x (MeV)	J^π [a]	ε_{TH1} [b]	ε_{TH2} [b]	$\sigma_\alpha^*/\sigma_\alpha^0$ [c]	
				TH1	TH2
0	0^+	$N = 34$	$N = 51$	1.28	1.43
1.97	2^+	2.2	0.9	1.33	1.39
4.18	3^-		1.1		1.25
4.33	$[0^+]$	8.10^3	33	0.5	1.18
4.44	$2^+(^{12}C^*)$ [d]	3.0	3.9	1.39	1.61
4.41	4^+ [e]	< 7	< 3	1.04	1.35
4.44	2^+			2.7	11
4.95	2_3^+	(270)	440	1.18	1.46
	2_4^+		(6)		1.15
5.17	5^-		0.6		1.23
5.19	$[0^+]$	(10^4)	390	1.44	1.3
5.84	1^- [e]		1.2		1.47
5.86	3^-				1.26
6.14	$[4_2^+]$	(260)	440	1.30	1.19
	$[4_3^+]$	(39)	3.5		
6.22	5^-		2.5		1.25
6.36	4_3^+	(2.7)	0.23	1.19	1.07
	4_2^+	(17)	29		

[a]) Spin-parity values in brackets are probable assignments from the present work. Lower-right indices indicate the sequence number of the J^π state in the calculation.

[b]) Enhancement factors (see eq. (5)) for calculations with the two sets of wave functions TH1 and TH2. Eight dominant terms in the cluster expansion were included in the DWBA calculations. For the ground-state transition the overall normalization factors N are given. Values in parentheses were calculated with wave functions of theoretical levels for which the identification with the experimental level is uncertain.

[c]) Ratio of cross sections calculated with eight dominant cluster terms and with only the ($q = 0$, $j_\alpha = 0^+$) terms.

[d]) State of ^{12}C.

[e]) Unresolved doublets.

cross sections is given in table 5. The ratio $\sigma_\alpha^*/\sigma_\alpha^0$ shows that the cross sections for the extended calculations ($\sigma_\alpha{}^*$) are in general about 10 to 50% larger than those which include the ($q = 0$, $j_\alpha = 0$) components only (σ_α^0). Only for the weak 4.44 MeV 2^+ state this ratio is larger than 2. The transition to the 4.33 MeV 0^+ state is the only case were a clear destructive interference of the individual components was found (with the TH1 model) leading to $\sigma_\alpha{}^*/\sigma_\alpha{}^0 = 0.5$. The stronger components tend to add up constructively in the transfer amplitudes.

From these calculations it can be concluded that the usual assumption of the 0s relative motion for the four nucleons transferred in the (^{16}O, ^{12}C) reaction is acceptable with a confidence level of about 50% for strongly excited states. Clearly the inclusion of excited clusters can not explain the large deviations from the

DWBA prediction found for some of the states excited in the $^{32}S(^{16}O, ^{12}C)^{36}Ar$ reaction.

5. Summary and conclusions

Accurate angular distributions were obtained with the $^{32}S(^{16}O, ^{12}C)^{36}Ar$ reaction for most of the excited states in ^{36}Ar, which are bound with respect to α-decay. Both the shape of the angular distributions and the magnitude (relative to the ground state) of the cross sections for all bound negative-parity states and for the low-energy positive-parity states were satisfactorily explained by standard DWBA calculations. In these calculations surface-transparent potentials have been used and form factors with spectroscopic amplitudes determined from shell-model calculations in a configuration space which allowed for excitation of one or two particles to the fp-shell. Large deviations, both in shape and in relative magnitude, from the standard DWBA calculations were found for the angular distributions of transitions to the second and third 0^+ states at 4.33 and 5.19 MeV, for the third 2^+ state at 4.95 MeV and for the second 4^+ state at 6.14 MeV, although for the latter state the identification with a theoretical level is somewhat ambiguous. Also the observed cross section for the first 2^+ state in ^{12}C excited in the reaction on ^{32}S is a factor of 4 larger than calculated.

In addition angular distributions were obtained for some α-unbound states in the region 6.5 – 8.5 MeV. Calculated angular distributions for these transitions deviate strongly from the observed shape, although especially for the 1^- states the dominant features can be recognized including a rise at larger angles.

Despite extensive searches, a better description of the deviating angular distributions could not be obtained by using modified optical potentials of the standard volume Woods-Saxon type, nor with L-dependent absorption. The real parts of the potentials were not investigated as thoroughly as the imaginary parts, but several classes of commonly used potentials were tried.

A more satisfactory description of the shapes of the angular distributions could be obtained by using bound-state wave functions with a steeper tail. However, a plausible way to obtain such wave fucntions, the inclusion of more deeply bound clusters in internally excited states, turned out to contribute insufficiently to the cross sections.

Some discrepancies between experimental and calculated angular distributions are also observed for the $(^{16}O, ^{12}C)$ reaction on other sd-shell targets. The most pronounced case is the 5.80 MeV 1^- state in ^{32}S, which deviates from the DWBA prediction both at 42 MeV 17) and at 60 MeV [18]) incident energy. The angular prediction both at 42 MeV [ref. [17])] and at 60 MeV [ref. [18])] incident energy. The angular distribution for the 3.78 MeV, 0^+ state in ^{32}S [ref. [17])] tends to show a discrepancy similar to that for the 0^+ states in ^{36}Ar, although the limited angular range

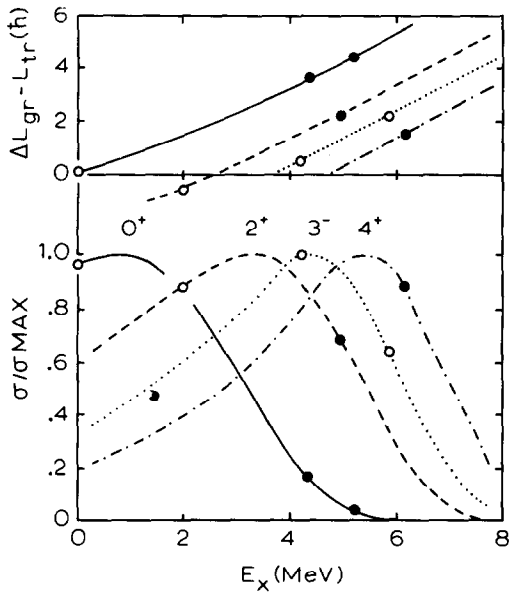

Fig. 10. Dynamical matching conditions for the reaction $^{32}S(^{16}O, ^{12}C)^{36}Ar$ leading to states of different spin and parity. The upper part of the figure gives the angular momentum mismatch, the difference of the grazing angular momenta in entrance and exit channel minus the transferred angular momentum, as a function of excitation energy in the final state. The lower part gives the Q-value dependence of the cross sections (calculated at forward angles). Solid, dashed, dotted and dot-dashed curves are for final states with $J^\pi = 0^+$, 2^+, 3^- and 4^+, respectively. Open circles indicate the position of states for which the experimental angular distributions are well reproduced by the DWBA calculations, whereas the full points are for transitions which are not described.

in the $^{24}Mg(^{16}O, ^{12}C)^{28}Si$ reaction [17]) are generally better described, but also there some angular distributions show more pronounced oscillations than reproduced by the DWBA calculation. All excited 0^+ states observed in these reactions have rather large spectroscopic factors, for which, however, no detailed shell-model calculations are available.

The dynamical conditions for the anomalous transitions and some normal transitions are given in fig. 10, calculated with the potentials used in the present analysis. It is found that the angular momentum mismatch for both 0^+ states is very large ($\Delta L_{gr} \approx 4$). For the 2^+ state at 4.95 MeV, $\Delta L_{gr} - L_{tr} \approx 2$ and for the 6.14 MeV 4^+ state $\Delta L_{gr} - L_{tr} = 1.5$. The optimum Q-values are found at $E_x = 1.0$, 3.5 and 5.5 MeV for states with $J = 0$, 2 and 4, respectively. Although the dynamical conditions are rather unfavourable for the 0^+ states, for the 2^+ and 4^+ states they are not worse than for the well-described negative-parity states. This suggests that the observed discrepancies should be related to special structure aspects or to the neglect of competing reaction mechanisms.

The resonance-like structures observed in the forward-angle excitation functions

of the (^{16}O, ^{12}C) reaction on ^{24}Mg[refs. [19-22])] and ^{28}Si[ref. [23])], although most thoroughly studied for the ground states, apparently exist also for the excited states [21]). These structures are highly correlated in all measured excitation functions. The amplitudes of the structures are rather large for the reaction on ^{24}Mg but decrease with increasing target mass (the peak-to-valley ratios for the reaction on ^{24}Mg and ^{28}Si are about 2 and 1.2, respectively). Thus there is no evidence for dominating isolated resonances in these reactions. To explain the large cross sections for the anomalous transitions in the ^{32}S(^{16}O, ^{12}C)^{36}Ar reaction in terms of resonances would require resonant amplitudes much larger than the direct background. However, an extrapolation of the observed trend for ^{24}Mg and ^{28}Si to ^{32}S makes such an explanation rather unlikely. Moreover the strong excitation of the same states in the (^{6}Li, d) reaction (see table 1), although measured only at one angle, points in the same direction.

The contribution of multi-step processes to transfer reactions with heavy ions has been discussed by Low [51]). Such processes may be expected to play a role in the excitation of collective states, involving inelastic excitation of target and/or projectile. Inelastic excitation of 0^+ states is, however, not very likely, because in general the lowest 2^+ and 4^+ states are the primary candidates to show effects of inelastic routes. In the present reaction these states behave normally. Moreover, no indication of strong population of excited 0^+ states in the inelastic scattering of ^{16}O on ^{32}S has been observed. Sequential transfer, often important for two-nucleon transfer reactions, is not likely to play a role in α-transfer reactions because of the unfavourable dynamical conditions for the intermediate channels resulting from the large separation energies.

For one-nucleon transfer reactions Delic *et al.* [52]) have discussed a mechanism involving polarization of shell-model states. This mechanism seems to explain systematic discrepancies observed for *L*- or *Q*-mismatched channels in one-nucleon transfer reactions, which are in some respect similar to those observed in the α-transfer reaction. To our knowledge no information about the effect of this mechanism on multi-nucleon transfer exists.

A more fascinating possibility is that the anomalous states contain configurations with four- (or even more) particle excitations to the fp-shell. In a rather simple model Strottman [53]) has predicted two almost degenerate states with one and two α-particles excited to the fp-shell at $E_x = 5$ MeV in ^{36}Ar. Such states may well have a strong clustering of α-particle strength at the nuclear surface, as was shown by Arima [54]) for excited 0^+ states in ^{20}Ne. The wave functions for such states are predicted to be very different in shape from the ground-state wave function. The usual procedure to generate the α-particle wave functions probably contains the most crude assumption of the DWBA formalism which is still open for discussion.

The authors wish to thank the technical staff of the tandem for the operation

of the machine, Mr. A. Michielsen for the preparation of the targets and Mr. E. van Meijgaard for his assistance with the analysis of the data.

This work was performed as part of the research program of the "Stichting voor Fundamenteel Onderzoek der Materie" (FOM) with financial support from the "Nederlandse Organisatie voor Zuiver-Wetenschappelijk Onderzoek" (ZWO).

References

1) A. Richter and C. Toepffer, in Heavy ion collisions, ed. R. Bock, vol. 1 (North-Holland, Amsterdam, 1979) p. 1
2) R. H. Siemssen, Int. Conf. on resonances in heavy ion reactions, Hvar, Yugoslavia, 1977
3) F. D. Becchetti, P. R. Christensen, V. I. Manko and R. J. Nickles, Nucl. Phys. **A203** (1973) 1
4) J. G. Cramer *et al.* Phys. Rev. **C14** (1976) 2158
5) G. R. Satchler *et al.*, Nucl. Phys. **A346** (1980) 179
6) J. Barrette and S. Kahana, Comm. Nucl. Part. Phys. **9** (1980) 67
7) A. J. Baltz and S. Kahana, Phys. Rev. **C17** (1978) 555
8) M. S. Chiou *et al.*, Phys. Rev. **C20** (1979) 851
9) C. M. Cheng *et al.*, Phys. Rev. **C20** (1979) 1042
10) P. Braun-Munzinger *et al.*, Phys. Rev. **C24** (1981) 1010
11) P. Braun-Munzinger *et al.*, Phys. Rev. Lett. **38** (1977) 944
12) C. K. Gelbke *et al.*, Phys. Rev. Lett. **41** (1978) 1778
13) M. R. Clover, B. R. Fulton, R. Ost and R. M. de Vries, J. of Phys. **G5** (1979) L63
14) M. Paul *et al.*, Phys. Rev. **C21** (1980) 1802
15) J. Barrette *et al.*, Phys. Rev. Lett. **40** (1978) 445
16) M. C. Mermaz *et al.*, Phys. Rev. **C24** (1981) 1512
17) J. C. Peng *et al.*, Nucl. Phys. **A264** (1976) 312
18) G. P. A. Berg *et al.*, Phys. Rev. **C19** (1979) 62
19) M. Paul *et al.*, Phys. Rev. Lett. **40** (1978) 1310
20) S. J. Sanders *et al.*, Phys. Rev. **C21** (1980) 1810
21) S. J. Sanders *et al.*, Phys. Rev. **C22** (1980) 1914
22) J. Nurzynski *et al.*, Nucl. Phys. **A363** (1981) 253
23) J. C. Peng *et al.*, Phys. Lett. **80B** (1978) 35
24) P. Braun-Munzinger and J. Barrette, Phys. Reports **87** (1982) 209
25) H. W. Fulbright and J. R. Erskine, Nucl. Instr. **162** (1979) 355
26) P. Braun-Munzinger *et al.*, Phys. Rev. Lett. **31** (1973) 1423
27) P. M. Endt and C. van der Leun, Nucl. Phys. **A310** (1978) 1
28) B. A. Lindgren *et al.*, Phys. Lett. **49B** (1974) 263
29) N. Austern, R. M. Drisko, E. C. Halbert and G. R. Satchler, Phys. Rev. **133** (1964) B3
30) D. Kurath and I. S. Towner, Nucl. Phys. **A222** (1974) 1
31) P. D. Kunz, computer code DWUCK5, unpublished
32) L. A. Charlton, Phys. Rev. **C8** (1973) 146
33) R. M. De Vries, computer code LOLA, unpublished
34) R. M. De Vries, G. R. Satchler and J. G. Cramer, Phys. Rev. Lett. **32** (1974) 1377
35) N. Austern, Direct nuclear reaction theories, (Wiley, New York, 1969)
36) J. R. Erskine *et al.*, Phys. Rev. Lett. **34** (1975) 680
37) M. -C. Lemaire, M. C. Mermaz, H. Sztark and A. Cunsolo, Proc. Conf. on reactions between complex nuclei, Nashville, 1974, ed. R. L. Robinson, F. K. McGowan, J. B. Ball and J. H. Hamilton (North-Holland, Amsterdam, 1974) p. 189
38) C. W. Glover *et al.*, Nucl. Phys. **A337** (1980) 520
39) W. Chung, thesis, Michigan State University, 1976, unpublished
40) C. J. van der Poel *et al.*, Nucl. Phys. **A394** (1983) 501
41) A. G. M. van Hees and P. W. M. Glaudemans, Nucl. Phys. **A396** (1983) 105c

42) D. Kurath, Phys. Rev. **C7** (1973) 1390
43) R. A. Chatwin, J. S. Eck, D. Robson and A. Richter, Phys. Rev. **C1** (1970) 795
44) T. Fliessbach, Z. Phys. **A288** (1978) 211
45) T. Fliessbach and P. Manakos, J. of Phys. **G3** (1977) 643
46) C. M. Vincent and H. T. Fortune, Phys. Rev. **C2** (1970) 782
47) R. Huby and J. R. Mines, Rev. Mod. Phys. **37** (1965) 406
48) R. Bock and H. Yoshida, Nucl. Phys. **A189** (1972) 177
49) C. L. Bennett, Nucl. Phys. **A284** (1977) 301
50) P. J. Brussaard and P. W. M. Glaudemans, Shell-model applications in nuclear spectroscopy (North-Holland, Amsterdam, 1977)
51) K. S. Low, J. de Phys. **37** (1976) C5-15
52) G. Delic, K. Pruess, L. A. Charlton and N. K. Glendenning, Phys. Lett. **69B** (1977) 20
53) D. Strottman, Phys. Lett. **36B** (1971) 321
54) A. Arima, in Heavy ion collisions, ed. R. Bock, vol. 1 (North-Holland, Amsterdam, 1979) p. 419